Impact of local vessel curvature on the circumferential plaque distribution in coronary arteries

Andreas Wahle,[a] Rubén Medina,[a,c] Kathleen C. Braddy,[b]
James M. Fox,[b] Theresa M. H. Brennan,[b] John J. Lopez,[b,d]
James D. Rossen,[b] and Milan Sonka[a]

The University of Iowa, [a]Department of Electrical and Computer Engineering,
and [b]Department of Internal Medicine, Iowa City, IA 52242, USA

[c]Universidad de Los Andes, Facultad de Ingeniería, Grupo de Ingeniería Biomédica,
Mérida 5101, Venezuela

[d]The University of Chicago, Department of Medicine, Chicago, IL 60637, USA

ABSTRACT

Plaque in native coronary arteries is hypothesized to accumulate more likely along the inner curvature of a vessel segment as compared to its outer curvature. This behavior is likely associated with differences in local shear stress, which tends to be lower on the inner bend of a curved vessel than on the outer bend. The reported in-vivo study evaluated how the circumferential plaque distribution depends on local vessel curvature in coronaries from a limited set of 12 patients. Geometrically correct models of the vessel segments were generated utilizing fusion between biplane angiography and intravascular ultrasound. The plaque thickness was derived from the 3-D borders of the lumen/plaque and media/adventitia interfaces. Within each frame, plaque thickness was classified into "below-average" and "above-average" regions. A local curvature index was defined for each point: A positive value indicates the "inner" curvature, a negative value the "outer" curvature, with the magnitude determined from differential geometry. In the majority of the examined vessels, regions of "below-average/outer-curvature" and "above-average/inner-curvature" combined outweighed the "below-average/inner-curvature" and "above-average/outer-curvature" regions. The ratio increased with the threshold to exclude lower-curvature regions, confirming the hypothesis that plaque is more likely to accumulate on the luminal surface along the inner curvature of the coronary segment.

Keywords: Coronary vessels, atherosclerosis, asymmetric plaque, intravascular ultrasound, X-ray angiography, 3-D multimodality fusion, differential geometry, vessel curvature

1. INTRODUCTION

Studying the progression of cardiovascular diseases as a function of local hemodynamics and plaque morphology in human vasculature is of increasing interest.[1,2] Frequently, plaque is not distributed homogeneously and tends to be circumferentially asymmetric (Fig. 1). There are certain indications that plaque in native coronary arteries is more likely to accumulate on the inner curvature of a vessel segment as compared to the outer curvature of the vessel, since the local wall shear stress tends to be lower on the inner bend of a curved vessel than on the outer bend (Fig. 2).[3–5] However, flow patterns and therefore the local shear-stress distribution are complex in tortuous vessel, as has been shown previously in large vessel such as the aorta.[6,7] The curved vessel segment can be considered as a collection of piece-wise toroidal sections. Wall points are located on the "inner" curvature if they are closer to the origin of the torus than the vessel centerline and on the "outer" curvature if they are farther from the origin than the centerline. Based upon differential geometry, a local curvature index can be defined for each point. Aim of this in-vivo study was to evaluate in a limited set of patients whether the circumferential plaque distribution actually depends on local vessel curvature.

E-mail: <andreas-wahle@uiowa.edu>; http://www.engineering.uiowa.edu/~awahle; Fax: +1-319-335-6028

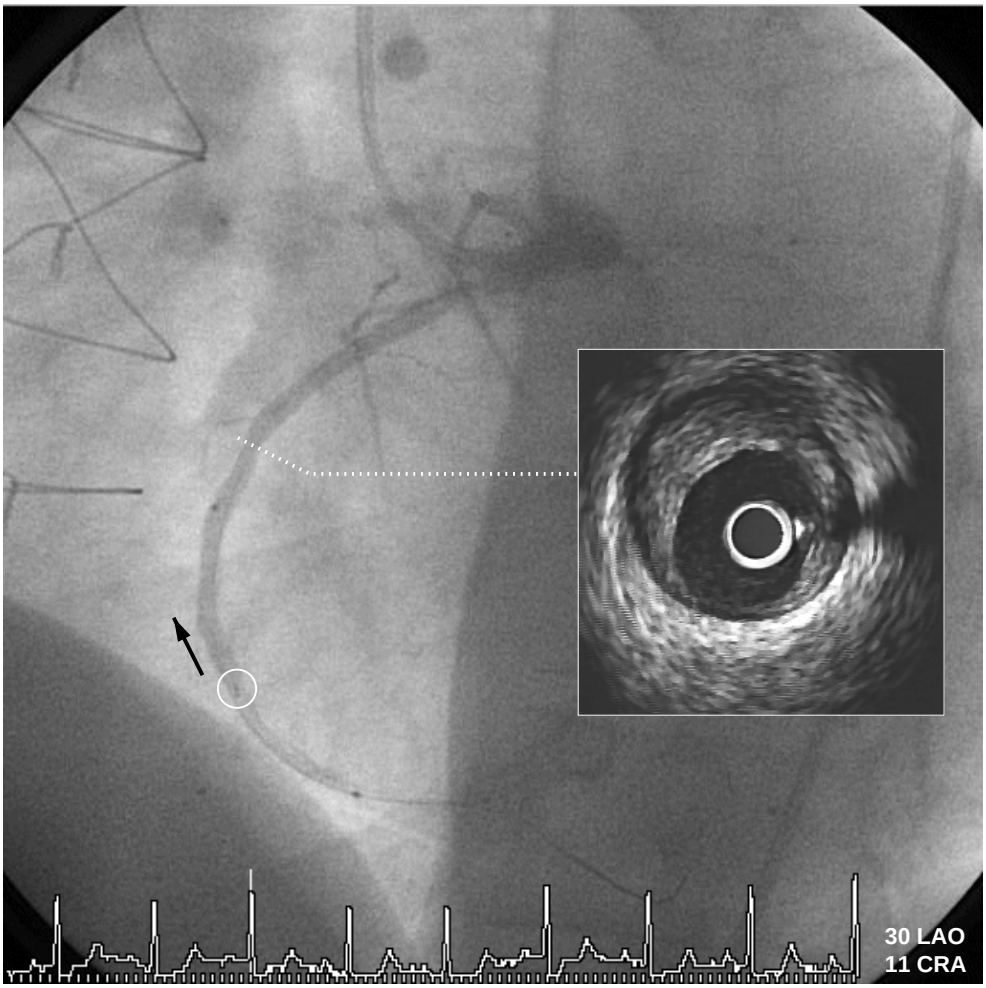

Figure 1. One of two biplane angiographic views showing an in-vivo imaged right coronary artery with the IVUS catheter inserted: While the angiogram can depict the lumen only, the IVUS image clearly demonstrates an asymmetric circumferential plaque distribution; the circle indicates the location of the IVUS transducer before the pullback starts, the arrow gives the direction of the motorized pullback.

2. METHODS

We have developed a fusion system that utilizes biplane angiography and intravascular ultrasound (IVUS) to generate a geometrically correct 3-D model of a vessel segment.[8–11] The processing pipeline starts with the acquisition of the angiographic and IVUS data from DICOM datasets and digitized S-VHS tapes, respectively, followed by segmentation of the data and finally the fusion itself. The resulting model is then analyzed for curvature and plaque distribution.

2.1. 3-D fusion

The 3-D vessel geometry is extracted from the angiograms whereas accurate cross-sectional information is obtained from IVUS. The IVUS transducer is placed well distally within the vessel segment of interest, its location imaged with biplane angiography, and then the catheter pulled back by an automated pullback device (Fig. 1). Using diluted contrast dye, the vessel lumen outline is also depicted in the angiograms and serves as a reference for the 3-D matching of the orientation of the IVUS frames. The resulting data are sorted by heart phase according to the ECG signal,[5] segmented for lumen/plaque and media/adventitia borders,[11] and then mapped into 3-D space based upon the angiographically determined pullback trajectory. The resulting model consists of

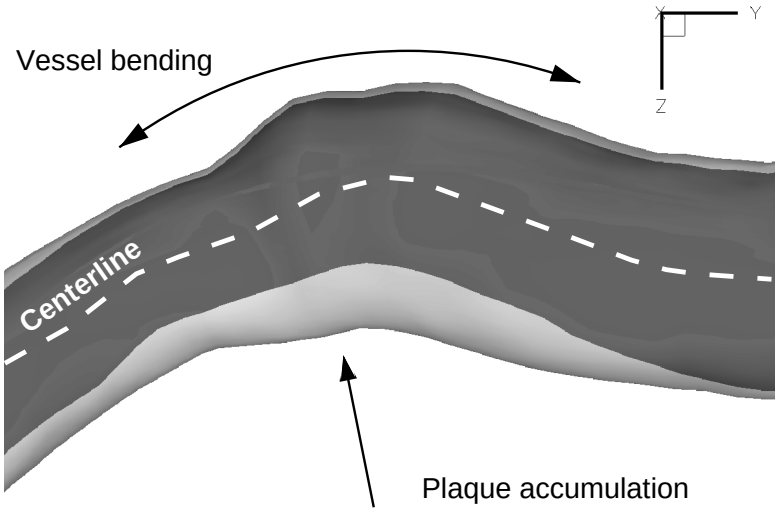

Figure 2. 3-D model derived from in-vivo patient data of a left anterior descending artery by fusion between biplane angiography and intravascular ultrasound: it can be clearly seen how the plaque accumulated inside the curvature.

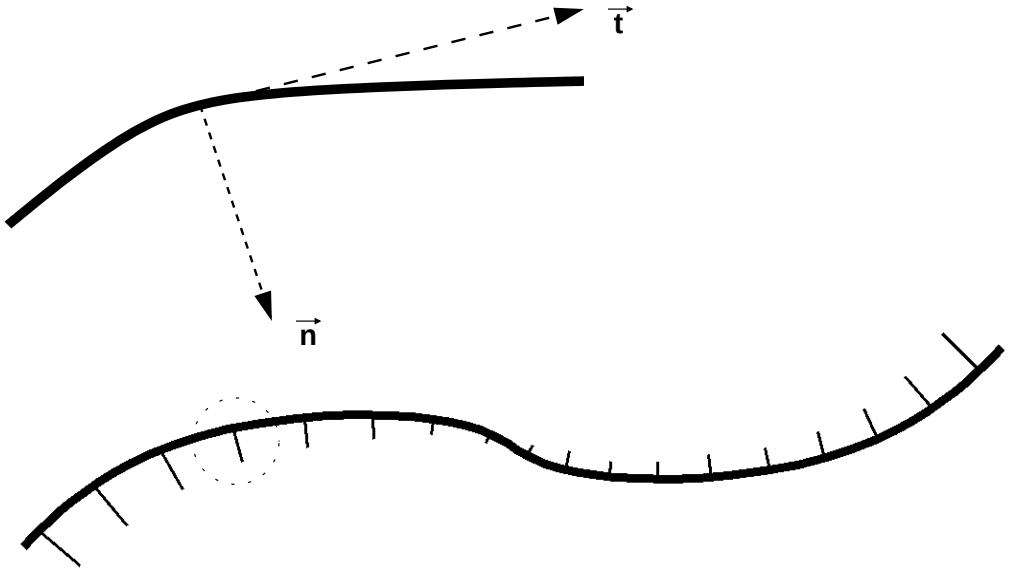

Figure 3. Definition of the local centerline tangent ($\vec{t}$) and normal ($\vec{n}$) vectors based upon the Frenet–Serret formulas.

a finite-element mesh that will be annotated by the plaque thickness and local curvature values. Other annotations may include the shear-stress results from computational hemodynamics,[5] morphological data such as local plaque volumes,[12] or radiation doses if intravascular brachytherapy was performed.[13]

2.2. Plaque-thickness analysis

The plaque thickness is directly derived from the two 3-D borders using radial lines connecting the vessel centroid to each contour point in each frame. Instead of the absolute thickness values, the plaque distribution is expressed relative to the average plaque thickness within each frame. Using the centroid rather than the location of the catheter ensures that the plaque thickness estimates are not distorted by the out-of-center position of the imaging catheter, as frequently seen.[8, 13] Connecting the centroids for each frame yields the centerline. These data are

derived from the lumen/plaque contour rather than the media/adventitia contour, thus the centroid is always located in the lumen (Fig. 2).

2.3. Local curvature and normal vectors

Calculating the curvature index requires first to determine the absolute curvature for each frame, and then to obtain a scalar signed value for each vertex point on the contours of each frame. The Frenet–Serret formulas[14, 15] deliver a set of three orthonormal unit vectors at any given point on a curved line, $\vec{t}$ (tangent), $\vec{n}$ (normal), and $\vec{b}$ (binormal). The curvature κ and the torsion τ are the angular velocities of the vectors $\vec{t}$ and $\vec{b}$, respectively, as the Frenet frame is moved along the centerline $c : [0, 1] \rightarrow \mathcal{R}^3$ at the relative position s over the pullback length:

$$\begin{aligned} c(s) &= [x(s), y(s), z(s)] \\ \kappa(s) &= \| c''(s) \| \\ \tau(s) &= \det[c'(s), c''(s), c'''(s)] \,/ \kappa^2(s) \end{aligned}$$

with $c'(s), c''(s), c'''(s)$ as the derivatives of c over the arc length s. Consequently, the derivatives of the three vectors, thus their relative changes from frame to frame of the pullback, calculate as follows:

$$\begin{aligned} \vec{t}\,'(s) &= +\kappa(s)\,\vec{n}(s) \\ \vec{n}\,'(s) &= -\kappa(s)\,\vec{t}(s) + \tau(s)\,\vec{b}(s) \\ \vec{b}\,'(s) &= -\tau(s)\,\vec{n}(s) \end{aligned}$$

where we are mainly interested in the normal vector $\vec{n}(s)$ for each frame, indicative of the direction, and the magnitude of the curvature $\kappa(s)$.

2.4. Determination of the curvature index

Applied to the centerline of a curved vessel segment, the normal vector will always point towards the origin of the radius of that curvature (Fig. 3). The magnitude of $\kappa(s)$ indicates the curvature strength while the direction of the normal $\vec{n}(s)$ can be used to determine the "inner" and "outer" curvatures on the circumference. In the first step, the unit normal vector $\vec{n}(s)$ is projected onto the local 2-D coordinate system of the IVUS frame located at s (Fig. 4). It has to be kept in mind that the absolute orientation of the IVUS frame set is virtually arbitrary (Fig. 5),[8] therefore the orientation of the IVUS frame cannot be used directly to determine the "inner" and "outer" curvatures.

Now, the direction of the "inner" curvature is known for all frames. However, $\vec{n}(s)$ is just a single vector derived from the centerline c for the frame located at s. What is obviously needed is to indicate for *each* contour point of the frame if it is located on the "inner" or the "outer" curvature or somewhere inbetween. The curvature magnitude $\kappa(s)$ has to be included as well. We defined a scalar curvature index $\kappa_{\mathrm{idx}}(s, i)$ that can be calculated for all points i of a contour s. A positive curvature index indicates "inner" curvature, a negative value "outer" curvature, and a value close to zero applies for points on the side of the curved vessel segment. The maximum positive curvature index and the minimum negative curvature index depend directly on the magnitude of the normal for that frame (Fig. 4). This approach was implemented by determining the unit vector from the centroid $\vec{c}(s)$ to the i-th point of the lumen contour in the IVUS frame $\vec{f}(s, i)$ and applying the dot-product:

$$\begin{aligned} \vec{v}(s, i) &= \vec{f}(s, i) - \vec{c}(s) \\ \kappa_{\mathrm{idx}}(s, i) &= \kappa(s)\vec{n}(s) \cdot \left(\frac{\vec{v}(s, i)}{||\vec{v}(s, i)||} \right) \end{aligned}$$

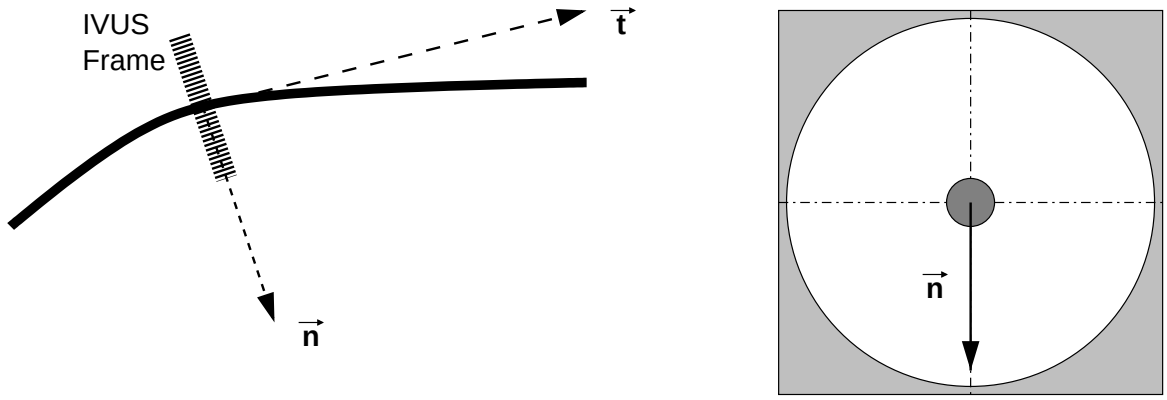

Figure 4. For each IVUS frame, the normal $\vec{n}$ is projected onto its plane as reconstructed in 3-D; this results in a frame-specific 2-D coordinate system determined by the orientation of $\vec{n}$ (for simplification, it is assumed here that the IVUS catheter is located in the centroid of the contour).

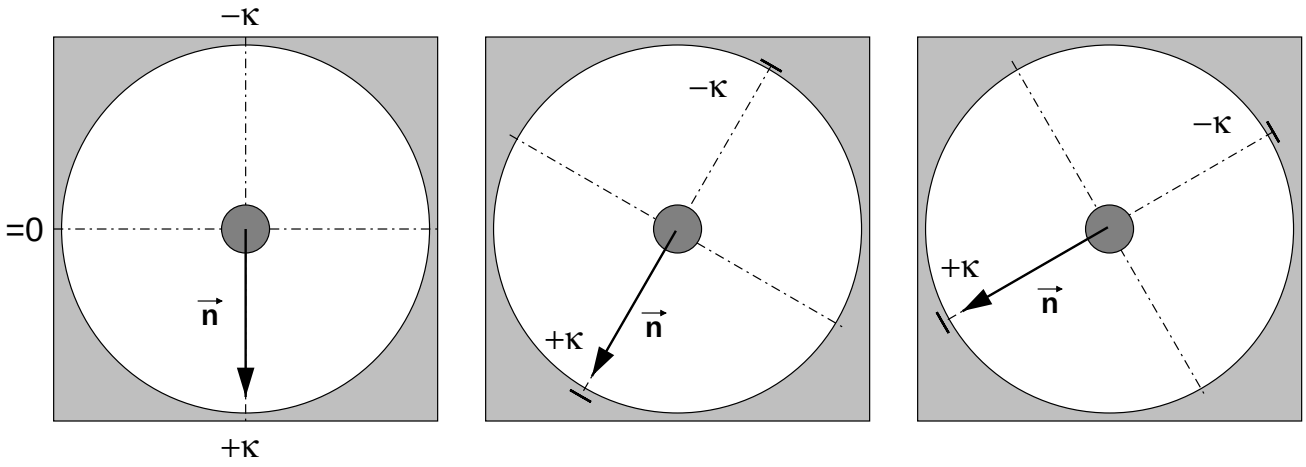

Figure 5. Definition of the *curvature index* to distinguish between "inner" and "outer" curvature: The absolute magnitude $|\kappa\vec{n}|$ is plotted as positive value on the locally inner curvature, whereas it is plotted as negative value on the locally outer curvature; contour elements perpendicular to $\vec{n}$ are zero and define "neutral" curvature.

2.5. Practical implications

Thus far it was assumed that $c(s)$ is continuous, which in practice is not the case. The 3-D finite-element mesh that was created during the fusion step is discrete in both radial and longitudinal dimensions. Instead of a continuous curve $c(s)$, a discretization by Δs needs to be taken into account. Therefore, a discrete version of the Frenet–Serret formulas was utilized. The second practical implication is the presence of noise, which is only partially resolved by smoothing of the finite-element mesh in both radial and longitudinal directions. Due to the distortions of the normal vectors, all $\vec{n}$ were smoothed in a moving $(23 \cdot \Delta s)$ window to obtain a more stable reference for the calculation of the curvature index. Finally, distorting influences, e.g., branching vessels, strong calcifications, or insufficient delineation of the media/adventitia border in stented areas had to be taken into account for the analysis. Therefore, these areas were identified visually, frame-wise marked as excluded, and no longer considered in the following analysis steps.

2.6. Definition of regions

After each contour point has been annotated with the local plaque thickness and the local curvature index, it is categorized into "below-average" if the plaque thickness is less than the average plaque thickness of the respective contour, "above-average" if the local plaque thickness is higher than the average, and secondly into "inner" or

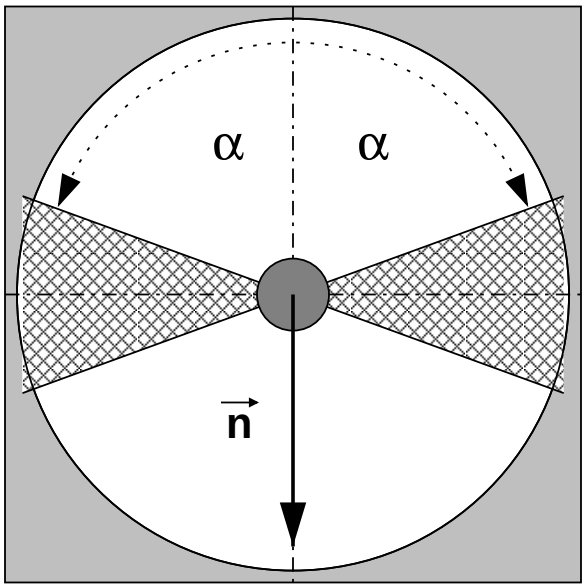

Figure 6. Definition of the exclusion threshold for "neutral" regions, shown here for the IVUS frame with maximum curvature magnitude $|\kappa|$; the angle α specifies the inclusion/exclusion ratio, where the threshold is determined by the $|\kappa|$-value at angle α relative to $\vec{n}$.

"outer" curvature depending on the sign of $\kappa_{\text{idx}}(s,i)$. This categorization results in four region types, i.e.:

$$\begin{aligned} R_{bo} &= \text{"below-average/outer-curvature"} \\ R_{bi} &= \text{"below-average/inner-curvature"} \\ R_{ao} &= \text{"above-average/outer-curvature"} \\ R_{ai} &= \text{"above-average/inner-curvature"} \end{aligned}$$

with a fifth region R_n = "neutral" added to indicate exclusions regions of low curvature. To determine if the curvature is below a certain threshold t, the maximum of the curvature for that specific vessel is multiplied with a factor derived from an exclusion angle (Fig. 6) by:

$$t = \max\{\kappa(s)\} \cdot \cos\alpha$$

2.7. Plaque-distribution vs. curvature ratio

For the hypothesis to hold, the combination of the R_{bo} and R_{ai} regions indicating "below-average/outer-curvature" and "above-average/inner-curvature" should outweigh both R_{bi} and R_{ao} combined, the "below-average/inner-curvature" and "above-average/outer-curvature" regions. A ratio r is calculated to indicate the relative number of elements that satisfy the hypothesis and which are not in any "neutral" region R_n:

$$r = \frac{R_{bo} + R_{ai}}{R_{bo} + R_{bi} + R_{ao} + R_{ai}}$$

therefore $r \geq 0.5$ implying that $(R_{bo} + R_{ai}) \geq (R_{bi} + R_{ao})$.

3. RESULTS

Thus far, the analysis has been performed in 12 arteries covering all three major coronary vessels. The vessel length was 72±20 mm with 5,040–16,776 pairs of lumen/plaque and media/adventitia border points. Curvature

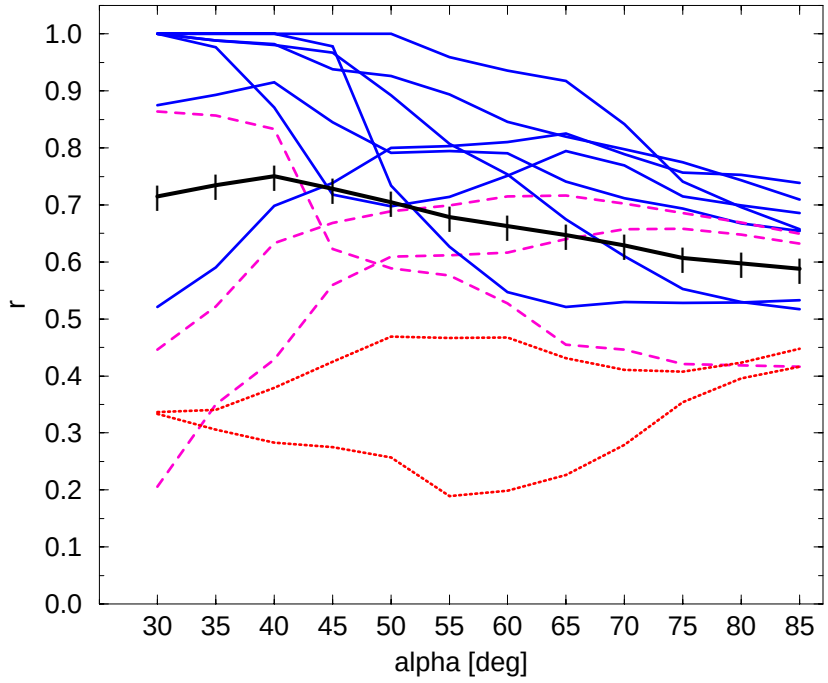

Figure 7. Ratio r as a function of α for all 12 patients, as well as the average (line with markers); solid lines mark vessels for which $r \geq 0.5$ is true for all α, dashed lines mark those for which $r < 0.5$ is true for *some* α, and dotted lines indicate that $r < 0.5$ is true for *all* α.

indices were calculated from the lumen/plaque borders. The ratio r was calculated separately for all vessels using $\alpha \in [30°, 85°]$ in 5° increments. On average over all 12 examined vessels, r increased from 0.588 for the lowest exclusion region ($\alpha = 85°$) to 0.715 for the highest number of excluded elements ($\alpha = 30°$). This shows that in the overall set, $r \geq 0.5$ was given, thus confirming the hypothesis for all thresholds in the testing range. Importantly, r shifted significantly towards the favorable R_{bo} and R_{ai} combinations with an increase of the curvature threshold t. There was however a substantial variance in result between patients (Fig. 7).

In 7 of the 12 examined vessels, $r \geq 0.5$ was given for all α thresholds, thus confirming the hypothesis unrestrictedly. An example from this subset is shown in Figs. 8/9. Another patient with a very tortuous vessel satisfied $r \geq 0.5$ only for all $\alpha \leq 60°$, yet showing an increase in r with an increase of t. In 2 patients, $r \geq 0.5$ was satisfied for $\alpha \geq 40°$ and $\alpha \geq 30°$, thus showing an actual decrease of r with an increase of t for high thresholds, while confirming the hypothesis in the vast majority of the tested thresholds. There were only 2 patients for which $r \geq 0.5$ could not be satisfied for any α within the testing range: both vessels were branches of the left anterior descending and left circumflex arteries, respectively, with a not well delineated angiographic appearance and with a poor IVUS quality due to calcification and stenting. This may have introduced inaccuracies in both IVUS segmentation[5] and the mapping of the data into 3-D by unresolved ambiguities in the determination of the absolute IVUS frame orientation.[8] In one of these patients, a ratio $r \geq 0.5$ could be achieved for $\alpha \geq 40°$ if only the native portion of the vessel segment (18.5 mm out of 55 mm pullback) was considered.

4. DISCUSSION

Our study showed that the hypothesis that circumferential plaque distribution is biased towards the inner curvature of a bent vessel was valid for averaged values over all patients as well as in the majority of vessels individually. While this is encouraging, and in accordance with in-vitro experiments,[3–5] the set of 12 patients

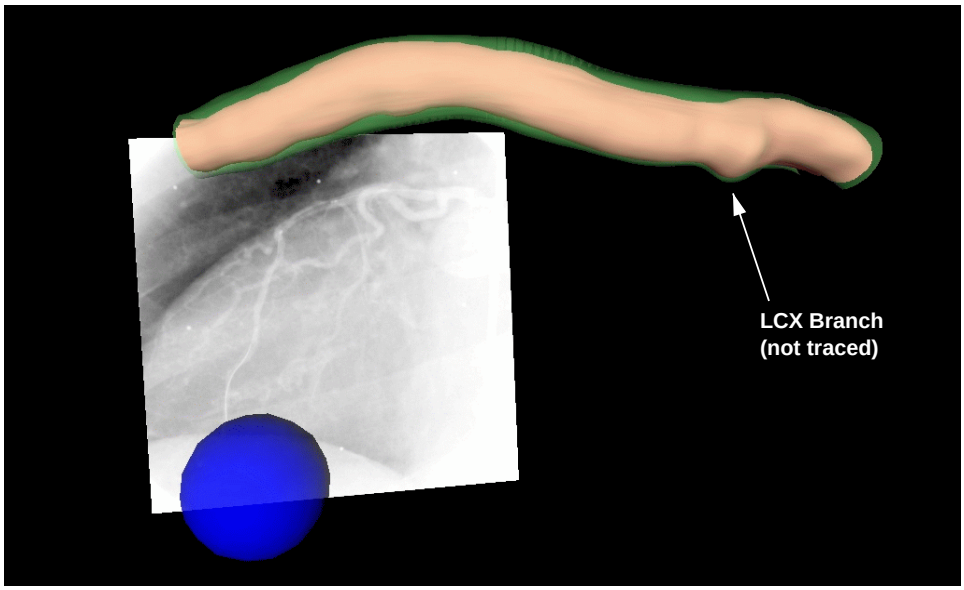

Figure 8. 3-D reconstruction of a slightly curved vessel segment (proximal left anterior descending artery with part of the left main), where the media/adventitia border is represented in a transparent green color.

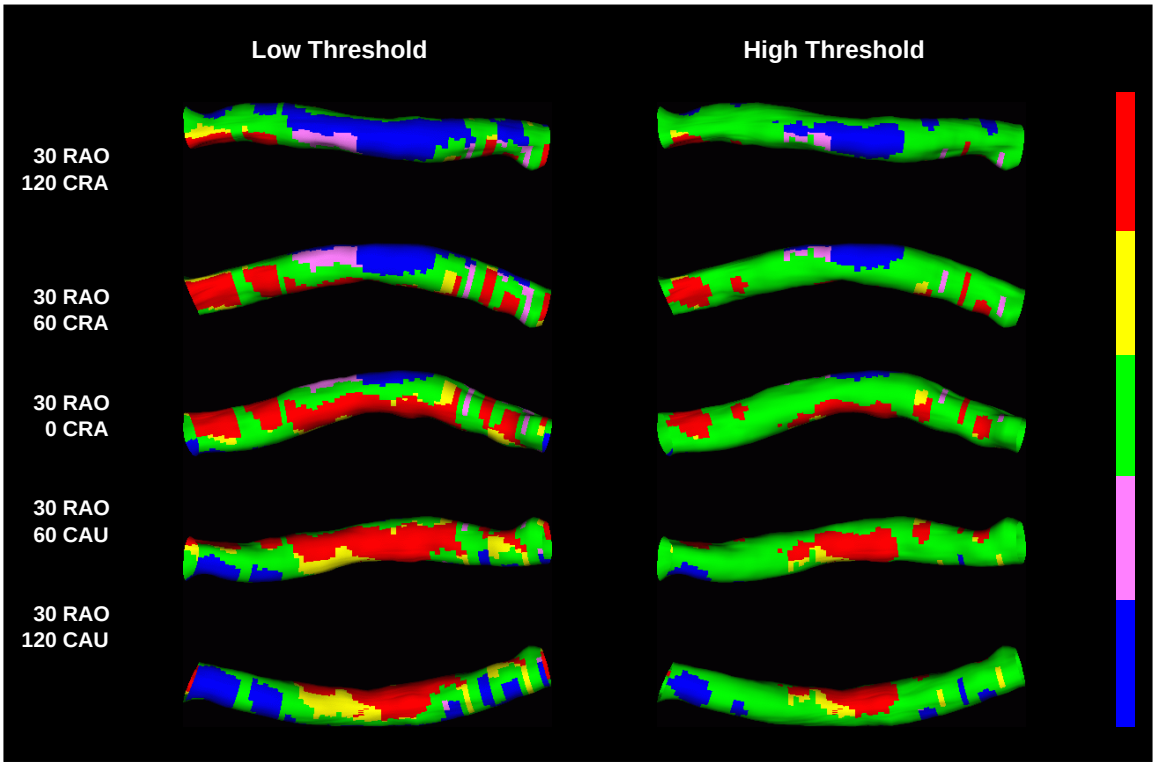

Figure 9. Assignment of regions for $\alpha = 75°$ (left, $R_n = 42.18\%$, $r = 0.775$) and $\alpha = 60°$ (right, $R_n = 74.42\%$, $r = 0.846$); region definition top down on right scale: **red** = R_{ai}, **yellow** = R_{bi}, **green** = R_n, **magenta** = R_{ao}, **blue** = R_{bo}.

(these figures are available in color on the CD version or on the authors' web page)

provided limited data and is expanded continuously to obtain a more conclusive set of analyses suitable for a statistic evaluation.

The analysis should preferably be performed in native vessel segments, since interventions (PTCA and stenting) seem at least to some degree to distort the relationship between plaque distribution and curvature. The vessels showing the worst results were usually small in diameter, were relatively straight, and/or had a large amount of calcifications or stented segments. It has to be evaluated at which point a vessel should be excluded for the study for these reasons, to ensure that the overall results are not distorted. Vessels with a non-trivial geometry and high non-planar tortuosity have a complex flow pattern that may superimpose the initial effect of circumferential plaque distribution towards the inner curvature.[6,7] Nevertheless, even the most tortuous vessel in our set basically confirmed the hypothesis.

Additional distortions may be introduced by the imaging and fusion process, e.g., the contour sampling is currently done perpendicularly to the IVUS catheter, which may not be in parallel with the vessel centerline. Consequently, the contour may represent an oblique slice cut through the vessel. These errors are assumed to be small and will be corrected soon by a resampling of the contours orthogonal to the vessel centerline. For the categorization into the regions, the threshold t is selected individually for each vessel from the maximum curvature $\kappa(s)$. We have also tested other ways to determine the threshold, e.g., over the entire set of vessels instead of individually for each vessel, or by using mean plus standard deviation ($\overline{\kappa} + \sigma_\kappa$) as factor for the threshold. While the individual values of r changed, the overall tendency remained stable.

5. CONCLUSIONS

In conclusion, preliminary results in a limited set of patients suggest that the common hypothesis of plaque accumulating on the inner curvature of a bent vessel holds. The actual quantification of a highly localized curvature index may allow a better prediction of sites of future plaque accumulation. Further improvement of the reconstruction and morphological-analysis techniques along with correlation with the local wall shear stress in these vessels will contribute to a better understanding of the mechanics behind plaque development.

ACKNOWLEDGMENTS

This work was supported in part by grant R01 HL63373 of the Heart, Lung, and Blood Institute at NIH, Bethesda, MD 20892, USA. Dr. Medina was supported by the Universidad de Los Andes and CONICIT (Venezuela) during his 2001–2002 academic year stay at The University of Iowa. The authors also would like to thank Steven C. Mitchell and Mark E. Olszewski, graduate students in Electrical and Computer Engineering at The University of Iowa, for their contributions to the development of the image data fusion system for geometrically correct reconstruction of coronary arteries in vivo.

REFERENCES

1. C. M. Gibson, L. Diaz, K. Kandarpa, F. M. Sacks, R. C. Pasternak, T. Sandor, C. L. Feldman, and P. H. Stone, "Relation of vessel wall shear stress to atherosclerosis progression in human coronary arteries," *Arteriosclerosis and Thrombosis* **13**, pp. 310–315, Feb. 1993.
2. R. Krams, J. J. Wentzel, J. A. F. Oomen, R. Vinke, J. C. H. Schuurbiers, P. J. de Feyter, P. W. Serruys, and C. J. Slager, "Evaluation of endothelial shear stress and 3-D geometry as factors determining the development of atherosclerosis and remodeling in human coronary arteries in-vivo; combining 3-D reconstruction from angiography and IVUS (ANGUS) with computational fluid dynamics," *Arteriosclerosis, Thrombosis and Vascular Biology* **17**, pp. 2061–2065, Oct. 1997.
3. Y. C. Agrawal, L. Talbot, and K. Gong, "Laser anemometer study of flow development in curved circular pipes," *Journal of Fluid Mechanics* **85**(3), pp. 497–518, 1978.
4. A. Santamarina, E. Weydahl, J. M. Siegel, and J. E. Moore, "Computational analysis of flow in a curved tube model of the coronary arteries: Effects of time-varying curvature," *Annals of Biomedical Engineering* **26**, pp. 944–954, Nov. 1998.

5. A. Wahle, S. C. Mitchell, S. D. Ramaswamy, K. B. Chandran, and M. Sonka, "Four-dimensional coronary morphology and computational hemodynamics," in *Medical Imaging 2001: Image Processing*, M. Sonka and K. M. Hanson, eds., **4322**, pp. 743–754, SPIE Proceedings, (Bellingham WA), 2001.
6. P. J. Kilner, G. Z. Yang, R. H. Mohiaddin, D. N. Firmin, and D. B. Longmore, "Helical and retrograde secondary flow patterns in the aortic arch studied by three-directional magnetic resonance velocity mapping," *Circulation* **88**, pp. 2235–2247, Nov. 1993.
7. H. Fujioka and K. Tanishita, "Numerical analysis of blood flow in the non-planar aortic arch model," in *Proc. 2001 ASME Bioengineering Conference*, **BED-50**, pp. 503–504, American Society of Mechanical Engineers, 2001.
8. A. Wahle, G. P. M. Prause, C. von Birgelen, R. Erbel, and M. Sonka, "Automated calculation of the axial orientation of intravascular ultrasound images by fusion with biplane angiography," in *Medical Imaging 1999: Image Processing*, K. M. Hanson, ed., **3661**, pp. 1094–1104, SPIE Proceedings, (Bellingham WA), 1999.
9. A. Wahle, G. P. M. Prause, S. C. DeJong, and M. Sonka, "Geometrically correct 3-D reconstruction of intravascular ultrasound images by fusion with biplane angiography — methods and validation," *IEEE Transactions on Medical Imaging* **18**, pp. 686–699, Aug. 1999.
10. A. Wahle, G. P. M. Prause, C. von Birgelen, R. Erbel, and M. Sonka, "Fusion of angiography and intravascular ultrasound in-vivo: Establishing the absolute 3-D frame orientation," *IEEE Transactions on Biomedical Engineering — Biomedical Data Fusion* **46**, pp. 1176–1180, Oct. 1999.
11. A. Wahle, S. C. Mitchell, M. E. Olszewski, R. M. Long, and M. Sonka, "Accurate visualization and quantification of coronary vasculature by 3-D/4-D fusion from biplane angiography and intravascular ultrasound," in *European Biomedical Optics Week (EBiOS 2000): Biomonitoring and Endoscopy Technologies*, I. Gannot, Y. V. Gulyaev, T. G. Papazoglou, and C. F. P. van Swol, eds., **4158**, pp. 144–155, SPIE Europto, (Bellingham WA), 2000/2001.
12. R. Medina, A. Wahle, M. E. Olszewski, and M. Sonka, "Volumetric quantification of coronary arteries reconstructed by fusion between intravascular ultrasound and biplane angiography," in *Proc. 2002 IEEE International Symposium on Biomedical Imaging*, pp. 891–894, IEEE Press, (Piscataway NJ), 2002.
13. A. Wahle, J. J. Lopez, E. C. Pennington, S. L. Meeks, K. C. Braddy, J. M. Fox, T. M. H. Brennan, J. M. Buatti, J. D. Rossen, and M. Sonka, "Estimating the actual dose delivered by intravascular coronary brachytherapy using geometrically correct 3-D modeling," in *Medical Imaging 2003: Visualization, Image-Guided Procedures, and Display*, R. L. Galloway, ed., **5029**, SPIE Proceedings, (Bellingham WA), 2003.
14. B. O'Neill, *Elementary Differential Geometry*, Academic Press, New York, 1966.
15. G. E. Farin, *Curves and Surfaces for Computer Aided Geometric Design: A Practical Guide*, Academic Press, Boston, 2nd ed., 1990.